Interaction of the mycotoxin metabolite dihydrocitrinone with serum albumin

Zelma Faisal,[1,2] Virág Vörös,[1] Beáta Lemli,[2,3,4] Diána Derdák,[3,4] Sándor Kunsági-Máté,[2,3,4] Mónika Bálint,[5] Csaba Hetényi,[5] Rita Csepregi,[2,6] Tamás Kőszegi,[2,6] Dominik Bergmann,[7] Franziska Sueck,[7] Hans-Ulrich Humpf,[7] Florian Hübner,[7] Miklós Poór [1,2,*]

[1]Department of Pharmacology, University of Pécs, Faculty of Pharmacy, Szigeti út 12, Pécs 7624, Hungary

[2]János Szentágothai Research Center, University of Pécs, Ifjúság útja 20, Pécs 7624, Hungary

[3]Department of Pharmaceutical Chemistry, University of Pécs, Faculty of Pharmacy, Rókus u. 2, Pécs 7624, Hungary

[4]Department of General and Physical Chemistry, University of Pécs, Ifjúság útja 6, Pécs 7624, Hungary

[5]Department of Pharmacology and Pharmacotherapy, Medical School, University of Pécs, Szigeti út 12, Pécs 7624, Hungary

[6]Department of Laboratory Medicine, University of Pécs, Medical School, Ifjúság útja 13, Pécs 7624, Hungary

[7]Institute of Food Chemistry, Westfälische Wilhelms-Universität Münster, Corrensstr. 45, 48149 Münster, Germany

*Corresponding author: Miklós Poór, PharmD, PhD
Department of Pharmacology, University of Pécs, Faculty of Pharmacy, Szigeti út 12, 7624 Pécs, Hungary
Phone: +36-72-536-000 / 35052
Fax: +36-72-536-218
E-mail address: poor.miklos@pte.hu

Abstract

Citrinin (CIT) is a nephrotoxic mycotoxin produced by *Penicillium*, *Monascus*, and *Aspergillus* species. CIT appears as a contaminant in cereals, cereal-based products, fruits, nuts, and spices. During the biotransformation of CIT, its major urinary metabolite dihydrocitrinone (DHC) is formed. Albumin interacts with several compounds (including mycotoxins) affecting their tissue distribution and elimination. CIT-albumin interaction is known; however, the complex formation of DHC with albumin has not been reported previously. In this study, we aimed to investigate the interaction of DHC with albumin, employing fluorescence spectroscopy, circular dichroism, and molecular modeling studies. Furthermore, species differences and thermodynamics of the interaction, as well as the effects of albumin on the acute *in vitro* toxicity of DHC and CIT were also tested. Our main observations/conclusions are as follows: (1) Fluorescence signal of DHC is strongly enhanced by albumin. (2) Formation of DHC-albumin complexes are supported by both fluorescence spectroscopic and circular dichroism studies. (3) DHC forms similarly stable complexes with human albumin ($K \sim 10^5$ L/mol) as CIT. (4) DHC-albumin interaction did not show significant species differences (tested with human, bovine, porcine, and rat albumins). (5) Based on modeling studies and investigations with site markers, DHC occupies the Heme binding site (subdomain IB) on human albumin. (6) The presence of albumin significantly decreased the acute *in vitro* cytotoxic effects of both DHC and CIT on MDCK cell line.

Keywords: Dihydrocitrinone; Citrinin; Serum albumin; Fluorescence spectroscopy; Albumin-ligand interaction

Introduction

Citrinin (CIT; Fig. 1) is a nephrotoxic mycotoxin produced by filamentous fungi, including *Penicillium*, *Monascus*, and *Aspergillus* genera (de Oliveira Filho et al., 2017). CIT appears as a contaminant in cereals, cereal-based products, fruits, nuts, and spices (Bennett and Klich, 2003; de Oliveira Filho et al., 2017). Several CIT-producing fungi are used in food industry during the production of cheese or some Asian foods. *Monascus purpureus* is applied even nowadays as a natural food colorant, despite the fact that it commonly produces CIT (da Rocha et al., 2014). The frequent occurrence of CIT in food was likely responsible for the "yellow rice toxins" syndrome/disease in Japan (1971) (Ciegler and Bennett, 1980). Antibacterial activity of CIT has also been reported because some Gram-positive bacteria are sensitive to CIT; however, it is not used in the pharmacotherapy due to its nephrotoxic effect in humans and animals (de Oliveira Filho, et al., 2017). Based on our current knowledge, the chronic CIT exposure may play a role in the development of endemic nephropathy in pigs and in human (Flajs and Peraica, 2009; Peraica et al., 2008). After oral exposure, CIT is extensively biotransformed in humans, during which its major urinary metabolite, dihydrocitrinone (DHC; Fig. 1) is formed (Ali et al., 2015; Huybrechts et al., 2014; Gerding et al. 2015; Degen et al., 2018). Based on previous reports, DHC appears in a wide concentration range in human blood and urine samples (0.00-1.44 ng/mL and 0.01-2.75 ng/mL, respectively) (Ali et al., 2015; Huybrechts et al., 2014; Gerding et al., 2015; Ali et al., 2018). The conversion of CIT to DHC is known as a detoxification reaction, due to the production of the more polar and less toxic metabolite. *In vitro* cellular toxicity and genotoxicity of DHC is significantly lower compared to the parent compound (Dunn et al., 1983; Föllmann et al., 2014). Under acidic conditions, CIT expresses strong fluorescence (λ_{ex} = 330 nm; λ_{em} = 505 nm); however, fluorescence signal of CIT strongly decreases with the

elevation of the pH and disappears approximately at pH 5, due to the deprotonation of the molecule (Poór et al., 2016).

Human serum albumin (HSA) is the most abundant protein in the human circulation. HSA maintains the oncotic pressure of the blood and displays buffering, antioxidant, and pseudo-enzymatic activities (Fanali et al., 2012). HSA forms stable complexes with several endogenous and exogenous compounds (Fanali et al., 2012; Yamasaki et al., 2013). HSA consists of three domains (I, II, and III), each domain is built up from two subdomains (A and B). The most important binding sites on HSA are Sudlow's site I (subdomain IIA) and Sudlow's site II (subdomain IIIA); however, recent studies draw the attention to the importance of Heme binding site (subdomain IB) (Fanali et al., 2012; Zsila, 2013). The interaction of CIT with HSA and with albumins from other species has been described (Damodaran, 1977; Damodaran and Shanmugasundaram, 1978; Poór et al., 2015); on the other hand, the DHC-albumin complex formation has not been reported. CIT binds to HSA with similar affinity to the oral anticoagulant warfarin (K = 2 x 10^5 L/mol), and its binding site is located in Sudlow's site I (Poór et al., 2015).

In this study, the complex formation of DHC with albumin was investigated employing fluorescence spectroscopy, circular dichroism, and molecular modeling. Stability of formed DHC-albumin complexes were evaluated based on the fluorescence quenching effect of DHC on albumins. Furthermore, binding constants were also determined, based on the fluorescence enhancement of DHC by albumins. To test the potential species differences, interaction of DHC with human, bovine (BSA), porcine (PSA), and rat (RSA) serum albumins was investigated. To get a deeper insight into the DHC-HSA complex formation, circular dichroism and thermodynamic studies were performed. Binding site of DHC on HSA was evaluated based on modeling studies and experiments with site markers. Finally, to

investigate the influence of albumin on the cellular uptake of the mycotoxin, acute toxicity of DHC and CIT was tested in MDCK kidney cell line, in the absence and presence of albumin.

Materials and Methods

Reagents

All reagents and solvents were of analytical or spectroscopic grade. The chemical synthesis of (±)-dihydrocitrinone (DHC, MW = 266.25 g/mol) was carried out according to the synthetic procedure for (±)-[$^{13}C_3$]-dihydrocitrinone described by Bergmann et al. (Bergmann et al., 2018), while (+)-DHC was purchased from AnalytiCon Discovery (Potsdam, Germany). As the natural metabolite (+)-DHC has only limited availability, most studies were performed with synthetic (±)-DHC and only the circular dichroism experiments with (+)-DHC. Citrinin (CIT, MW = 250.25 g/mol), human serum albumin (HSA, MW = 66.4 kDa), bovine serum albumin (BSA, MW = 66.4 kDa), porcine serum albumin (PSA, MW = 67.5 kDa), rat serum albumin (RSA, MW = 64.6 kDa), ochratoxin A (MW = 403.8 g/mol), warfarin (WAR, MW = 308.33), phenylbutazone (MW = 308.37 g/mol), furosemide (MW = 330.74 g/mol), ibuprofen (MW = 206.28 g/mol), methyl orange (MW = 327.34 g/mol), bilirubin (MW = 584.66 g/mol), zearalenone (MW = 318.36 g/mol), L-thyroxine (MW = 776.87 g/mol), and Dulbecco's Modified Eagle Medium (DMEM) were purchased from Sigma-Aldrich. Fetal bovine serum (FBS, from Pan-Biotech) and Bioluminescent ATP Assay Kit CLSII (from Roche) were used as received. Stock solution of DHC (2500 µmol/L, 0.666 g/L), CIT (2500 µmol/L, 0.626 g/L), ochratoxin A (5000 µmol/L, 2.019 g/L), zearalenone (5000 µmol/L, 1.592 g/L), ibuprofen (2500 µmol/L), furosemide (2500 µmol/L), phenylbutazone (2500 µmol/L), warfarin (2500 µmol/L), and L-thyroxine (2500 µmol/L)were prepared in 96 v/v% ethanol (Renal, spectroscopic grade); while methyl orange (2000 µmol/L) and bilirubin (500 µmol/L) were dissolved in dimethyl sulfoxide (Fluka, spectroscopic grade). Stock solutions were stored at -

20 °C protected from light. To mimic extracellular physiological conditions, measurements were carried out in phosphate-buffered saline (PBS: 8.00 g/L NaCl, 0.20 g/L KCl, 1.81 g/L $Na_2HPO_4 \times 2H_2O$, 0.24 g/L KH_2PO_4; pH 7.4).

Spectroscopic measurements

Steady-state fluorescent spectroscopic and fluorescence anisotropy measurements were carried out employing a Hitachi F-4500 fluorescence spectrophotometer (Tokyo, Japan). Analyses were performed at 25 °C (except thermodynamic studies) in the presence of air. In order to exclude the inner filter effect, UV-Vis spectra of DHC, CIT, warfarin, phenylbutazone, furosemide, ibuprofen, methyl orange, bilirubin, zearalenone, and L-thyroxine were also recorded, applying a Specord Plus 210 (Analytic Jena AG, Jena, Germany) spectrophotometer. Fluorescence emission intensities were corrected with the following equation (Hu and Liu, 2015):

$$I_{cor} = I_{obs} * e^{(A_{ex}+A_{em})/2} \quad (1)$$

where I_{cor} and I_{obs} denote the corrected and observed fluorescence emission intensities, respectively; while A_{ex} and A_{em} are the absorbance values of compounds (DHC, CIT ibuprofen, warfarin, phenylbutazone, furosemide, methyl orange, bilirubin, zearalenone, L-thyroxine) at the excitation and emission wavelengths used, respectively.

During fluorescence quenching studies, increasing concentrations of DHC (0.0, 0.5, 1.0, 2.0, 3.0, and 4.0 μmol/L; 0.00-1.07 mg/L range) were added to standard amount of albumin (2 μmol/L) in PBS (pH 7.4). Quenching experiments were evaluated based on the Stern-Volmer equation (Hu and Liu, 2015):

$$\frac{I_0}{I} = 1 + K_{SV} * [Q] \quad (2)$$

where I_0 and I are fluorescence intensities of albumin without and with DHC, respectively (λ_{ex} = 295 nm, λ_{em} = 340 nm), K_{SV} is the Stern-Volmer quenching constant (unit: L/mol), while $[Q]$ is the concentration of the quencher (unit: mol/L).

Binding constants (K) of DHC-albumin complexes were determined by non-linear fitting, using the Hyperquad2006 program package (Protonic Software), during which the following equations were implemented in the Hyperquad code (SA: serum albumin) (Faisal et al., 2018):

$$pSA + qDHC \leftrightarrow SA_pDHC_q \quad (3)$$

$$\beta_{pq} = \frac{[SA_pDHC_q]}{[SA]^p[DHC]^q} \quad (4)$$

where p and q indicate the stoichiometry of the equilibrium in the solution. In Hyperquad2006 computer fitting program all equilibrium constants were defined as overall binding constants (see below).

$$SA + DHC \leftrightarrow SA\,DHC \qquad \beta_1 = \frac{[SA\,DHC]}{[SA][DHC]} \quad (5)$$

$$SA + qDHC \leftrightarrow SA\,DHC_q \qquad \beta_q = \frac{[SA\,DHC_q]}{[SA][DHC]^q} \quad (6)$$

The relationship between the overall binding constants and the stepwise binding constants were calculated by the Hyperquad based on the followings.

$$\beta_1 = K_1;\ \ \beta_q = K_1 \times K_2 \ldots \times K_q \quad (7)$$

The stoichiometry and binding constant of DHC-albumin complexes were determined using the model associated with the lowest standard deviation.

Fluorescence spectra of DHC and DHC-albumin complexes were recorded applying 325 and 405 nm as excitation and emission wavelengths, respectively. Increasing albumin concentrations (0, 0.5, 1.0, 1.5, 2.0, 3.0, 4.0, 5.0, 6.0, 8.0, 10.0, 12.5, and 15.0 μmol/L) were added to standard amount of DHC (2 μmol/L, 0.533 mg/L) in PBS (pH 7.4). Binding constants were determined by the Hyperquad2006 software (see Eqs. 3-7).

To investigate the displacement of DHC from HSA by site markers, increasing concentrations of ibuprofen, phenylbutazone, furosemide, methyl orange, bilirubin, zearalenone, and L-thyroxine (0, 1, 2, 4, and 6 μmol/L each) were added to standard amount of DHC and HSA (2 and 4 μmol/L, respectively). Fluorescence emission spectra were recorded in PBS (pH 7.4) using the wavelength maximum of DHC-albumin complexes (λ_{ex} = 325 nm, λ_{em} = 405 nm). Since the complex formation of DHC with albumin results in significant enhancement of the fluorescence of the mycotoxin metabolite, displacement of DHC from HSA leads to the significant decrease of its fluorescence signal.

Thereafter, the influence of DHC (vs. CIT and warfarin) on the fluorescence anisotropy of ochratoxin A-HSA complex was examined using the previously described method (Poór et al., 2015). Increasing concentrations of DHC, CIT, and warfarin (0-30 μmol/L each) were added to standard amounts of ochratoxin A and HSA (1 μmol/L and 1.5 μmol/L, respectively) in PBS (pH 7.4). Then fluorescence anisotropy values of these samples were determined using 394 and 447 nm as excitation and emission wavelengths, respectively (wavelength maxima of albumin-bound ochratoxin A). Fluorescence anisotropy (*r*) data were calculated employing the following equation (Lakowicz, 2006):

$$r = \frac{(I_{VV} - G \times I_{VH})}{(I_{VV} + 2 \times G \times I_{VH})} \qquad (8)$$

where *G* is the instrumental factor, I_{VV} and I_{VH} are emission intensities measured in vertical position of polarizer at pre-sample site, and at vertical and horizontal position of post-sample polarizer, respectively.

Circular dichroism

The circular dichroism spectra of (+)-DHC were measured at room temperature using a 1 cm cell with a Jasco J-600 CD spectrometer (Jasco, Groß-Umstadt, Germany). The spectra were recorded between 200-270 nm with 1 nm step size, 1 nm bandwidth, 100 nm/min speed and

an average time of 0.5 s. Five measurements from each sample were performed and averaged without using the smoothing function. Two different DHC concentrations (0.48 µmol/L = 0.128 mg/L and 0.96 µmol/L = 0.256 mg/L) were incubated in duplicates with 0.48 µmol/L HSA in 30 mmol/L phosphate buffer (4.4 g/L Na_2HPO_4, 0.6 g/L KH_2PO_4, pH was adjusted to 7.4 with 0.1 mol/L H_3PO_4) for 5 h at room temperature while shaking. The same HSA solution at a concentration of 0.48 µmol/L (determined by Bradford assay) was used for all experiments. Ellipticity (θ_{MRE}) was used for converting the observed ellipticity (θ_{obs}) to the mean residue based on the following equation:

$$\theta_{MRE} = \frac{\theta_{obs}}{10 \text{ x } C_p \text{ x } n \text{ x } l} \quad (9)$$

where C_p is the protein concentration (4.8 x 10^{-7} mol/L), n is the number of amino acids of HSA (584) and l is the length of the cuvette (1 cm). For the calculation of the α-helix percentage, the following equation was employed, and software K2D3 was utilized (Wang et al., 2013; Ajmal et al., 2017; Louis-Jeune et al., 2012).

$$\text{α-helix (\%)} = \frac{-\theta_{\text{MRE 208nm}} - 4000}{33000 - 4000} \text{ x } 100 \quad (10)$$

For the K2D3 software the θ_{MRE} from 200-240 nm and the protein size of 584 amino acids were applied.

Thermodynamic studies

To get a deeper insight into the DHC-HSA interaction, thermodynamic parameters were determined, during which binding constants of complexes were calculated at six different temperatures (298, 301, 304, 307, 310, and 313 K). Binding constants (K) were quantified based on fluorescence spectroscopic measurements employing the Hyperquad2006 software (see Eqs. 3-7), using 325 and 405 nm excitation and emission wavelengths, respectively. Thermodynamic parameters associated to the complex formations between DHC and HSA were determined using the van't Hoff equation:

$$logK = -\frac{\Delta G}{RT} = -\frac{\Delta H}{2.303 \times R \times T} + \frac{\Delta S}{2.303 \times R} \quad (11)$$

where *ΔG, ΔH*, and *ΔS* reflect the Gibbs free energy, enthalpy, and entropy changes of the binding reaction, respectively; while *R* refers to the gas constant and *T* is the temperature.

Modeling studies

The ligand structure was built in Maestro (Schrödinger, 2017). The raw structure was energy minimized, using the semi-empirical quantum chemistry program package, MOPAC (Stewart, 1990) and the PM6 parameterization (Stewart, 2007). The gradient norm was set to 0.001. The energy minimized structure was subjected to force calculations. The force constant matrices were positive definite. The minimized ligand structures were then used in our docking calculations.

An apo crystallographic structure (PDB code: 1ao6) of HSA was used as target molecule in our calculations. Acetyl and amide capping groups were attached to the N- and C-termini, respectively, using the Schrödinger Maestro program package v. 9.6 (Schrödinger, 2017). As 1ao6 contains a homodimer structure, only chain A was used for calculations. Co-crystallized ions and water molecules were removed before minimizing the protein structure. The target molecule was minimized using a two-step protocol with the GROMACS software package (Abraham et al., 2015), including a steepest descent and a conjugate gradient step, and using AMBER99-ildn force field (Lindorff-Larsen et al., 2010). Exit tolerance levels were set to 1000 and 10 kJ mol^{-1} nm^{-1} while maximum step sizes were set to 0.5 and 0.05 nm, respectively. The minimized target was then used in our docking calculations.

Using the optimized ligand and target structures, blind docking calculations were performed with AutoDock 4.2 program package (Morris et al., 2009) as described in our previous publications (Poór et al., 2015; Hetényi and van der Spoel, 2002, 2006, 2011). Gasteiger-Marsilli partial charges were added to both the ligand and target atoms, using AutoDock

Tools (Morris et al., 2009) and united atom representation was applied for non-polar moieties. A grid box of 250 × 250 × 250 points, and 0.375 Å spacing was calculated and centered on target center of mass by AutoGrid 4. Lamarckian genetic algorithm was used for global search. Flexibility was allowed on the ligand at all active torsions, number of docking runs was set to 100, numbers of energy evaluations and generations were 20 million (Hetényi and van der Spoel, 2006). Ligand conformations that resulted from the docking runs were ordered by the corresponding calculated interaction energy values and subsequently clustered using a tolerance of 1.75 Å root mean square deviation (RMSD) between cluster members (Hetényi and van der Spoel, 2002).

Cell cultures and ATP-based cell viability assay

MDCK (Madin-Darby canine kidney epithelial cells, ATCC: CCL-34) adhesion cell line was cultured in DMEM supplemented with 10% FBS, penicillin (100 U/mL), and streptomycin (100 μg/mL), in a humidified atmosphere (5% CO_2) at 37 °C. Trypsinized cells were plated in 96-well plastic plates (approximately 10^4 cells/well). Before the treatment, the culture medium was replaced with fresh one (without FBS/HSA, with FBS, or with HSA), then cells were incubated with 50 μmol/L (DHC: 13.313 mg/L; CIT: 12.513 mg/L) or 100 μmol/L (DHC: 26.625 mg/L; CIT: 25.025 mg/L) mycotoxin concentrations in the absence and in the presence of 10% FBS or 40 g/L HSA. After 24-h incubation, ATP levels were quantified applying the previously described method without any modifications (Sali et al., 2016).

Statistics

Means and standard error (± SEM) values expressed in figures. Statistical evaluation of experiments with site markers and *in vitro* cell experiments were carried out using one-way

ANOVA test (IBM SPSS Statistics, Version 21), during which the level of significance was set at $p < 0.05$ and $p < 0.01$.

Results and Discussion

Fluorescence spectroscopic investigation of DHC in the absence and presence of HSA

First, the fluorescence excitation and emission spectra of DHC were recorded in PBS (pH 7.4). Despite the parent compound (CIT) does not express fluorescence at physiological pH (Poór et al., 2016), conversion of CIT to DHC leads to significant spectral changes. As Fig. S1 demonstrates, DHC showed fluorescence property in PBS, exerting its excitation and emission wavelength maxima at 325 and 420 nm, respectively.

Because interaction of fluorophores with albumin can lead to changes in their fluorescence (Sueck et al., 2018), the influence of HSA on the fluorescence emission spectrum of DHC was tested. Increasing amounts of HSA (final concentrations: 0-15 μmol/L) were added to DHC (2 μmol/L) in PBS, then emission spectra were recorded (λ_{ex} = 325 nm). In a dose dependent fashion, HSA caused a significant fluorescence enhancement of DHC, during which the blue shift of the emission wavelength maximum of DHC (420 → 405 nm) was noticed (Fig. 2a). Under the applied conditions, HSA also shows some fluorescence emission; however, the increase in fluorescence resulted from the presence of HSA is relatively low (Fig. 2b). Considering the highest molecular orbital of DHC, the aromatic moiety takes part in the fluorescence process through two ways: (a) the interaction of the aromatic ring in DHC with the surface of albumin modifies the fluorescence efficiency of the aromatic moiety; (b) the partial removal of water molecules from the solvation shell of DHC, prior its interaction with the albumin, enhances the fluorescence of DHC due to the reduced number of the quencher water molecules in the solvation shell. These observations strongly suggest the formation of DHC-HSA complexes. Since the increased fluorescence at 405 nm is partly

originating from the fluorescence signal of HSA, emission intensities were corrected during the calculation of binding constants (see later in *Binding constants of DHC-albumin complexes* section).

Fluorescence quenching of HSA by DHC

Fluorescence emission spectrum of HSA (2 μmol/L) was recorded in PBS (pH 7.4), in the absence and presence of increasing concentrations of DHC (0-4 μmol/L; λ_{ex} = 295 nm, λ_{em} = 340 nm). Using 295 nm as excitation wavelength, HSA shows emission maximum at 340 nm, while a second peak at higher wavelength (approximately at 405 nm) also appears in the presence of DHC, due to the fluorescence emission of DHC and DHC-HSA complex (Fig. 3a). In a concentration dependent fashion, DHC induced the decrease of the fluorescence signal at 340 nm as a result of the fluorescence quenching effect of DHC on HSA. To exclude the inner-filter effect, fluorescence signal of HSA was corrected based on Eq. 1. The good linearity of the Stern-Volmer plot (R^2 = 0.993) recommends 1:1 stoichiometry of complex formation. The decrease in the slope of the Stern-Volmer plot at higher temperature values suggests the static quenching process of HSA by DHC (see below in the *Thermodynamics of DHC-HSA complex formation* section).

Binding constants of DHC-albumin complexes

In order to evaluate the stability of DHC-albumin complexes and the potential species differences of DHC-albumin interactions, experiments described in the previous two sections were performed with bovine (BSA), porcine (PSA), and rat (RSA) serum albumins. Similarly to HSA, other albumins also induced the significant fluorescence enhancement of DHC (Fig. S2). The strongest enhancers were HSA and RSA causing approximately 75-fold increase in the fluorescence of DHC, while the less effective enhancers BSA and PSA led to the 60-fold

and 25-fold elevation of fluorescence, respectively. Fluorescence quenching effect of DHC was the highest in the presence of RSA, followed by HSA and BSA, while the lowest decrease of fluorescence was observed with PSA (Fig. 3b).

Quantitation of binding constants were determined using both models: (a) enhancement of the fluorescence of DHC by albumins (Fig. S2), and (b) quenching the fluorescence of albumins by DHC (Fig. 3). Decimal logarithmic values of Stern-Volmer quenching constants (K_{SV}; unit: L/mol) and binding constants (K; unit: L/mol) are demonstrated in Table 1 for each examined DHC-albumin complexes. The logK_{SV} values determined based on the Stern-Volmer equation (Eq. 2) were in a good correlation with the log$K$ values calculated using the Hyperquad program (Eqs. 3-7). The quenching model suggests somewhat lower binding constants compared to the other approach; however, the tendencies of species differences are similar in both models. DHC forms the most stable complex with RSA, followed by HSA, BSA, and PSA. The stability of DHC-RSA complex is approximately 4-5 times higher compared to DHC-PSA, however, only moderate species differences were observed during the comparison of the binding constant of DHC-HSA with other DHC-albumin complexes. Albumin-binding of some mycotoxins shows large species-dependent differences, for example ochratoxin A and zearalenone/zearalenols (Faisal et al., 2018). From this point of view, DHC behaves very similarly to the parent compound CIT; the latter binds to HSA with almost the same affinity (log$K$ = 5.32) and shows similar species differences to DHC (Poór et al., 2015).

Circular dichroism (CD) of HSA with DHC

CD is a useful analytical tool for the characterization of the secondary structure of proteins as the absorption of the circularly polarized light between 200 and 240 nm provides information on the percentage of α-helices and β-sheets of a protein (Wang et al., 2013). Based on the limited availability of the natural isomer (+)-DHC, it was examined only in CD experiments

342 (other studies were performed with (±)-DHC). In order to recognize changes in the secondary
343 structure of HSA in the presence of (+)-DHC, CD-spectra of the single compounds and their
344 mixture were recorded in the 200-270 nm range. For the CD experiments, a 0.48 μmol/L
345 concentration of HSA in 30 mmol/L phosphate buffer (pH 7.4) was used and for the
346 incubation of HSA with (+)-DHC at equimolar concentration. While (+)-DHC did not show a
347 CD effect, characteristic CD spectra for HSA and the mixture of HSA and (+)-DHC were
348 recorded (Fig. 4).
349 The mean residue ellipticity (θ_{MRE}) of the native HSA at the characteristic wavelength minima
350 of 208 nm and 222 nm indicate that the native protein had predominantly α-helix secondary
351 structure (Fig. 4). The characteristic minima that are indicative for the α-helices are caused by
352 amino acids of the protein (Wang et al., 2013). In the presence of DHC, a slight increase of
353 θ_{MRE} was observed at these characteristic wavelengths of 208 nm and 222 nm. These
354 observations suggest that the complex formation of DHC with HSA leads to a slight change in
355 the secondary structure of HSA, resulting in a decrease of α-helicity (Fig. 4). The native HSA
356 had α-helix percentage of 67.4 to 73.3% (Table 2). After incubation with DHC, the α-helicity
357 of HSA was reduced by 3-9%, suggesting the formation of DHC-HSA complexes. HSA (0.48
358 μmol/L) was also incubated with double equivalent concentration of DHC (0.98 μmol/L)
359 under the same conditions, during which no further increase of the θ_{MRE} was observed.
360
361 *Thermodynamics of DHC-HSA complex formation*
362 The temperature dependence of the binding constants of DHC-HSA complex was investigated
363 between 298 and 313 K. Similarly to the CIT-HSA complex (Poór et al., 2015), the log*K* values
364 of DHC-HSA show higher stability at lower temperatures, reflecting the presence of ground
365 state complexes. Fig. S3 demonstrates the van't Hoff plot of DHC-HSA complex, and the
366 thermodynamic parameters derived from the slope and the intercept of the line fitted to the log*K*

values (Eq. 11). ΔH and ΔS associated to the DHC-HSA complex formation were found to be -22.65 kJ mol^{-1} and +23.29 J K^{-1} mol^{-1}, respectively. The calculated negative ΔG value (-29.78 kJ mol^{-1}) suggests the spontaneous binding process between DHC and HSA at room temperature, and it is within the typical range of non-covalent interactions. These values are close to the parameters obtained for CIT-HSA interaction (ΔG = -29.96 kJ mol^{-1}, ΔH = -24.15 kJ mol^{-1}, and ΔS = 20.90 J K^{-1} mol^{-1}) (Poór et al., 2015). Thermodynamic data indicate similar binding characteristics of DHC-HSA and CIT-HSA complexes, namely electrostatic forces play a major role in the complex formation. According to the entropy gain of DHC-HSA interaction, it is reasonable to hypothesize the partial decomposition of the solvation shells of interacting molecules, leading to a less ordered structure of water molecules (Ross and Subramanian, 1981).

Modeling studies

Blind docking calculations resulted in 100 ligand conformations, which were further clustered as described in the *Materials and Methods* section. After clustering, five ligand conformations were obtained, which were ordered by the calculated interaction energy between the target and the ligand molecule. Out of the five clusters, the first four are illustrated in Fig. 5a, and discussed in the followings.

Each analyzed docking rank bound to known binding pockets (Fanali et al., 2012). The first rank (Rank 1) bound to the Sudlow's site I (binding site of the oral anticoagulant warfarin; Fig. S4a), the second rank (Rank 2) partially occupied the FA9 binding site (near to one of the binding sites of L-thyroxine; Fig. S4b), the third rank (Rank 3) bound to approximately 10Å distance from the binding site of mycotoxin zearalenone (Fig. S4c) (Faisal et al., 2018), and the fourth rank (Rank 4) bound to the Heme binding site (FA1; one of its typical ligands is bilirubin; Fig. S4d).

The binding conformation of Rank 4 DHC interacts with both hydrophobic (L115, I142) and hydrophilic (R114, H146, R145, R186, K190) amino acids in the Heme binding site (Fig. 5b). The DHC is secured in the Heme site through H-bonds and salt bridges between the hydrophilic amino acids and the carboxyl and hydroxyl groups of the DHC. The hydrophobic interactions act between L115 and I142 amino acids and the methyl groups of the DHC.

Investigation of the binding site of DHC on HSA using site markers

To examine the binding site of DHC on HSA, some typical ligands of Sudlow's site I (phenylbutazone and furosemide), Sudlow's site II (ibuprofen), and Heme binding site (bilirubin and methyl orange) were applied (Fanali et al., 2012; Zsila, 2013). Furthermore, to test the potential involvement of Rank 2 (FA9) or Rank 3 as binding sites, the effects of L-thyroxine and zearalenone on DHC-HSA interaction was also tested. In these experiments, our previous observation that albumin-binding significantly increases the fluorescence signal of DHC was utilized (Fig. 2). Using this principle, it is reasonable to hypothesize that the displacement of DHC from albumin leads to the significant decrease in its fluorescence at 405 nm (emission wavelength maximum of HSA-bound DHC). Therefore, fluorescence emission spectrum of DHC-HSA complex (2 and 4 μmol/L, respectively) was recorded in the presence of increasing concentrations of site markers (0, 1, 2, 4, and 6 μmol/L) in PBS (λ_{ex} = 325 nm). The concentrations of solvents did not exceed 1.2 v/v% which did not influence the fluorescence of DHC-HSA complex in the absence of site markers. As Fig. 6a demonstrates, the presence of L-thyroxine, zearalenone, and the markers of Sudlow's site I and II induced negligible changes in the fluorescence of DHC-HSA complex. On the other hand, both markers of the Heme binding site (methyl orange and bilirubin) significantly decreased the fluorescence at 405 nm, suggesting the displacement of DHC from HSA by these compounds, and the involvement of the Heme binding site regarding DHC-HSA interaction. The binding

417 constant of bilirubin-HSA complex is much higher compared to methyl orange-HSA (Ahlfors,
418 1981; Zsila, 2013), which is in agreement with our observation that bilirubin can induce
419 stronger displacement of DHC from HSA compared to methyl orange.
420 Previous investigations revealed that CIT occupies Sudlow's site I as its primary binding site
421 on HSA (Poór et al., 2015). Since the binding constant, the binding mode, and species
422 differences of DHC-albumin complex are very similar to the CIT-albumin complex, it is
423 surprising that DHC occupies another binding site than CIT. Thus, to confirm these results,
424 further experiments were performed with the known markers of site I, namely warfarin and
425 ochratoxin A (Il'ichev et al., 2002). During this experiment, our previously described model
426 was employed (Poór et al., 2015). Since ochratoxin A is a small fluorophore, its interaction
427 with the macromolecule (HSA) results in the significant decrease in its rotational freedom and
428 consequently the strong increase of fluorescence polarization or anisotropy values of the
429 mycotoxin. Based on these principles, albumin-binding of ochratoxin A can be precisely
430 followed by fluorescence polarization or anisotropy techniques (Poór et al., 2015).
431 Fluorescence anisotropy of ochratoxin A with HSA (1.0 and 1.5 μmol/L, respectively) were
432 determined in the presence of increasing concentrations of DHC, CIT, or warfarin (each 0, 1,
433 5, 10, 20, and 30 μmol/L). CIT and warfarin induced similar (but statistically not significant)
434 decrease in the fluorescence anisotropy of ochratoxin A, while DHC caused only a slight
435 effect (Fig. 6b). Since the decrease in fluorescence anisotropy is resulted from the increased
436 rotational freedom of ochratoxin A, this observation suggests the displacement of ochratoxin
437 A from HSA in the presence of CIT and warfarin. The fact that even relatively large
438 concentrations of DHC failed to significantly decrease the anisotropy value of ochratoxin A
439 supports our previous finding that the binding site of DHC is not located in Sudlow's site I.
440
441 *Influence of albumin on the acute cellular toxicity of DHC and CIT*

In order to examine the influence of albumin on the acute cellular toxicity of DHC and CIT, MDCK kidney cells were treated with these mycotoxins in the absence and presence of 10% FBS or 40 g/L HSA. Cell culture media usually contains 10% FBS (final concentration of BSA: approximately 3.5 g/L), while 40 g/L is a typical HSA concentration in the human blood. Since the acute cytotoxicity of DHC and CIT is relatively low, high mycotoxin concentrations (50 and 100 μmol/L) were applied to produce remarkable toxic effects. Each sample (including the control) contained the same ethanol concentrations (4 v/v%, which was the solvent of CIT and DHC). Mycotoxin-induced loss of cell viability was evaluated based on ATP levels/well after 24-h incubation. As Fig. 7 demonstrates, the applied mycotoxin concentrations caused significant decrease of ATP. In agreement with previous studies, the lower toxicity of DHC was observed compared to CIT (Föllmann et al., 2014). In the presence of FBS and HSA, the cytotoxicity of both CIT and DHC significantly decreased (Fig. 7), most likely due to the formation of stable mycotoxin-albumin complexes which can limit the cellular uptake of these mycotoxins. Stronger effect of HSA (vs. FBS) can be mainly attributed to the lower BSA concentration in the cell medium (3.5 g/L BSA vs. 40 g/L HSA). Therefore, our results demonstrate that the interaction of DHC with albumin may significantly affect the tissue uptake of the mycotoxin.

In conclusion, the interaction of DHC with albumin was investigated by fluorescence spectroscopy, circular dichroism, and molecular modeling. Binding constant and binding site, species-dependent alternations, and thermodynamics of the interaction were characterized, as well as the effects of albumin on the *in vitro* cytotoxicity of DHC and CIT were also tested. DHC exerts fluorescence signal at physiological conditions, which is strongly enhanced by albumin. Besides the increased fluorescence of DHC in the presence of albumins, the formation of DHC-albumin complexes is also supported by fluorescence quenching and circular dichroism studies. Stability of DHC-HSA, DHC-BSA, and DHC-PSA complexes

were similar, while DHC binds to RSA with slightly higher affinity compared to other albumins tested. Binding constant of DHC-HSA complex is similar to CIT-HSA; however, DHC occupies Heme binding site (FA1; subdomain IB) on HSA while CIT is a ligand of Sudlow's Site I (subdomain IIA). Thermodynamic studies suggest the spontaneous binding process between DHC and HSA at room temperature, during which electrostatic forces play a major role. Furthermore, the partial decomposition of the solvation shells can be assumed. Albumin decreased significantly the toxic effects of both DHC and CIT on MDCK cells, which also confirms the formation of stable mycotoxin-albumin complexes.

Source of Funding

This project was supported by the Hungarian National Research, Development and Innovation Office (FK125166) (M.P.) and the Deutsche Forschungsgemeinschaft (GRK1143, IRTG Münster-Nagoya) (H.H.). The work of M.B. and C.H. was supported by the Hungarian National Research, Development and Innovation Office (K123836).

Acknowledgements

This project was supported by the János Bolyai Research Scholarship of the Hungarian Academy of Sciences (M.P.). M.P. is thankful for support of the University of Pécs for grant in the frame of Pharmaceutical Talent Centre program. This work was supported by the GINOP-2.3.2-15-2016-00049 grant. This project was supported by the ÚNKP-18-2 New National Excellence Program of the Ministry of Human Capacities (V.V.). We acknowledge a grant of computer time from CSCS Swiss National Supercomputing Centre, and the Governmental Information Technology Development Agency, Hungary. We acknowledge that the results of this research have been achieved using the DECI resource Archer based in the UK at the National Supercomputing Service with support from the PRACE aisbl. The

University of Pécs is acknowledged for a support by the 17886-4/23018/FEKUTSTRAT excellence grant.

Conflict of interest: The authors declare no conflict of interest. We have full control of all primary data and we agree to allow the journal to review our data if requested.

References

Abraham MJ, Murtola T, Schulz R, Páll S, Smith JC, Hess B, Lindahl E (2015) GROMACS: high performance molecular simulations through multi-level parallelism from laptops to supercomputers. SoftwareX 1:19-25. https://doi.org/10.1016/j.softx.2015.06.001

Ahlfors CE (1981) Competitive interaction of biliverdin and bilirubin only at the primary bilirubin binding site on human albumin. Anal Biochem 110:295-307. https://doi.org/10.1016/0003-2697(81)90195-0

Ajmal MR, Nusrat S, Alam P, Zaidi N, Khan MV, Zaman M, Shahein YE, Mahmoud MH, Badr G, Khan RH (2017) Interaction of anticancer drug clofarabine with human serum albumin and human α-1 acid glycoprotein. Spectroscopic and molecular docking approach. J Pharm Biomed Anal, 135:106-115. https://doi.org/10.1016/j.jpba.2016.12.001

Ali N, Blaszkewicz M, Degen GH (2015) Occurrence of the mycotoxin citrinin and its metabolite dihydrocitrinone in urines of German adults. Arch Toxicol 89:573-578. https://doi.org/10.1007/s00204-014-1363-y

517

518 Ali N, Hossain K, Degen GH (2018) Blood plasma biomarkers of citrinin and ochratoxin A
519 exposure in young adults in Bangladesh. Mycotoxin Res 34:59–67.
520 https://doi.org/10.1007/s12550-017-0299-5
521

522 Bennett JW, Klich M (2003) Mycotoxins. Clin Microbiol Rev 16:497-516.
523 https://doi.org/10.1128/CMR.16.3.497–516.2003
524

525 Bergmann D, Hübner F, Wibbeling B, Daniliuc C, Cramer B, Humpf H-U (2018) Large-scale
526 total synthesis of $^{13}C_3$-labeled citrinin and its metabolite dihydrocitrinone. Mycotoxin Res
527 34:141-150.
528 https://doi.org/10.1007/s12550-018-0308-3
529

530 Ciegler A, Bennett JW (1980) Mycotoxins and Mycotoxicoses. BioScience 30:512-515.
531 https://doi.org/10.2307/1307970
532

533 da Rocha MEB, Freire FCO, Maia FEF, Guedes MIF, Rondina D (2014) Mycotoxins and
534 their effects on human and animal health. Food Control 36:59-165.
535 https://doi.org/10.1016/j.foodcont.2013.08.021
536

537 Damodaran C (1977) In vitro binding of citrinin to serum protein. Experientia 33:598-599.
538 https://doi.org/10.1007/BF01946519
539

540 Damodaran C, Shanmugasundaram E (1978) Distribution of radioactive citrinin in tissues and
541 serum protein(s). J Radioanal Chem 46:373-377.

https://doi.org/10.1007/BF02519903

Degena GH, Ali N, Gundert-Remy U (2018) Preliminary data on citrinin kinetics in humans and their use to estimate citrinin exposure based on biomarkers. Toxicol. Lett. 282:43-48. http://dx.doi.org/10.1016/j.toxlet.2017.10.006

de Oliveira Filho JWG, Islam MT, Ali ES, Uddin SJ, Santos JVO, de Alencar MVOB, Júnior ALG, Paz MFCJ, de Brito MDRM, e Sousa JMC, Shaw S, de Medeiros MDGF, Dantas SMMM, Rolim HML, Ferreira PMP, Kamal MA, Pieczynska MD, Das N, Gupta VK, Mocan A, Dos Santos Andrade TJA, Singh BN, Mishra SK, Atanasov AG, Melo-Cavalcante AAC (2017) A comprehensive review on biological properties of citrinin. Food Chem Toxicol 110:130-141. https://doi.org/10.1016/j.fct.2017.10.002

Dunn BB, Stack ME, Park DL, Joshi A, Friedman L, King RL (1983) Isolation and identification of dihydrocitrinone, a urinary metabolite of citrinin in rats. J Toxicol Environ Health 12:283-289. https://doi.org/10.1080/15287398309530426

Faisal Z, Lemli B, Szerencsés D, Kunsági-Máté S, Bálint M, Hetényi C, Kuzma M, Mayer M, Poór M (2018) Interactions of zearalenone and its reduced metabolites α-zearalenol and β-zearalenol with serum albumins: species differences, binding sites, and thermodynamics. Mycotoxin Res. 34:269-278. https://doi.org/10.1007/s12550-018-0321-6

Fanali G, di Masi A, Trezza V, Marino M, Fasano M, Ascenzi P (2012) Human serum albumin: From bench to bedside. Mol Asp Med 33:209-290. https://doi.org/10.1016/j.mam.2011.12.002

Flajs D, Peraica M (2009) Toxicological Properties of Citrinin. Arh Hig Rada Toksikol 60:457-464. https://doi.org/10.2478/10004-1254-60-2009-1992

Föllmann W, Behm C, Degen GH (2014) Toxicity of the mycotoxin citrinin and its metabolite dihydrocitrinone and of mixtures of citrinin and ochratoxin A in vitro. Arch Toxicol 88:1097-1107. https://doi.org/10.1007/s00204-014-1216-8

Gerding J, Ali N, Schwartzbord J, Cramer B, Brown DL, Degen GH, Humpf H-U (2015) A comparative study of the human urinary mycotoxin excretion patterns in Bangladesh, Germany and Haiti using a rapid and sensitive LC-MS/MS approach. Mycotoxin Res 31:127-136. https://doi.org/10.1007/s12550-015-0223-9.

Hetényi C, van der Spoel D (2002) Efficient docking of peptides to proteins without prior knowledge of the binding site. Protein Sci 11:1729-1737. https://doi.org/10.1110/ps.0202302

Hetényi C, van der Spoel D (2006) Blind docking of drug-sized compounds to proteins with up to a thousand residues. FEBS Lett 580:1447-1450.

https://doi.org/10.1016/j.febslet.2006.01.074

Hetényi C, van der Spoel D (2011) Toward prediction of functional protein pockets using blind docking and pocket search algorithms. Protein Sci 20:880-893. https://doi.org/10.1002/pro.618

Hu T, Liu Y (2015) Probing the interaction of cefodizime with human serum albumin using multi-spectroscopic and molecular docking techniques. J Pharm Biomed Anal 107:325-332. https://doi.org/10.1016/j.jpba.2015.01.010

Huybrechts B, Martins JC, Debongnie Ph, Uhlig S, Callebaut A (2015) Fast and sensitive LC–MS/MS method measuring human mycotoxin exposure using biomarkers in urine. Arch Toxicol 89:1993-2005. https://doi.org/10.1007/s00204-014-1358-8

Il'ichev YV, Perry JL, Simon JD (2002) Interaction of Ochratoxin A with Human Serum Albumin. A Common Binding Site of Ochratoxin A and Warfarin in Subdomain IIA. J Phys Chem B 106:460-465. https://doi.org/10.1021/jp012315m

Lakowicz JR (2006) Fluorescence Anisotropy In: Principles of Fluorescence Spectroscopy 3rd edn. Baltimore, Maryland, pp 353-382.

615 Lindorff-Larsen K, Piana S, Palmo K, Maragakis P, Klepeis JL, Dror RO, Shaw DE (2010)
616 Improved side-chain torsion potentials for the Amber ff99SB protein force field. Proteins
617 78:1950-1958.
618 https://doi.org/10.1002/prot.22711
619
620 Louis-Jeune C, Andrade-Navarro MA, Perez-Iratxeta C (2012) Prediction of protein
621 secondary structure from circular dichroism using theoretically derived spectra. Proteins
622 80:374-381.
623 https://doi.org/10.1002/prot.23188
624
625 Morris GM, Huey R, Lindstrom W, Sanner MF, Belew RK, Goodsell DS, Olson AJ (2009)
626 AutoDock4 and AutoDockTools4: automated docking with selective receptor flexibility. J
627 Comput Chem 30:2785-2791.
628 https://doi.org/10.1002/jcc.21256
629
630 Peraica M, Domijan AM, Miletic´-Medved M, Fuchs R (2008) The involvement of
631 mycotoxins in the development of endemic nephropathy. Wien Klin Wochen 120: 402-407.
632 https://doi.org/10.1007/s00508-008-0981-x
633
634 Poór M, Lemli B, Bálint M, Hetényi C, Sali N, Kőszegi T, Kunsági-Máté S (2015) Interaction
635 of citrinin with human serum albumin. Toxins 7:5155-5166.
636 https://doi.org/10.3390/toxins7124871
637

638 Poór M, Matisz G, Kunsági-Máté S, Derdák D, Szente L, Lemli B (2016) Fluorescence
639 spectroscopic investigation of the interaction of citrinin with native and chemically modified
640 cyclodextrins. J Lumin 172:23-28.
641 https://doi.org/10.1016/j.jlumin.2015.11.011
642
643 Ross PD, Subramanian S (1981) Thermodynamics of protein association reactions: forces
644 contributing to stability. Biochemistry 20:3096-3102.
645 https://doi.org/10.1021/bi00514a017
646
647 Sali N, Nagy S, Poór M, Kőszegi T (2016) Multiparametric luminescent viability assay in
648 toxicology models: a critical evaluation. J Pharmacol Toxicol Methods 79:45-54.
649 https://doi.org/10.1016/j.vascn.2016.01.004
650
651 Schrödinger LLC. (2017) New York, NY
652
653 Stewart JJ. MOPAC 2007 (2007) Version 7, 290 W. Stewart Computational Chemistry,
654 Colorado Springs, CO
655
656 Sueck F, Poór M, Faisal Z, Gertzen CGW, Cramer B, Lemli B, Kunsági-Máté S, Gohlke H,
657 Humpf H-U (2018) Interaction of ochratoxin A and its thermal degradation product 2'R-
658 ochratoxin A with human serum albumin. Toxins 10: E256.
659 https://doi.org/10.3390/toxins10070256
660
661 Wang Q, Yan J, He J, Bai K, Li H (2013) Characterization of the interaction between 3-
662 xotabersonine and two serum albumins by using spectroscopic techniques. J Lumin 138:1-7.

663 https://doi.org/10.1016/j.jlumin.2013.01.035
664
665 Yamasaki K, Chuang VT, Maruyama T, Otagiri M (2013) Albumin-drug interaction and its
666 clinical implication. Biochim Biophys Acta 1830:5435-5443.
667 https://doi.org/10.1016/j.bbagen.2013.05.005
668
669 Zsila F (2013) Subdomain IB Is the Third Major Drug Binding Region of Human Serum
670 Albumin: Toward the Three-Sites Model. Mol Pharmaceutics 10:1668-1682.
671 https://doi.org/10.1021/mp400027q

672 **List of figures:**

673

674 **Fig. 1** Chemical structures of citrinin and dihydrocitrinone

675

676 **Fig. 2 a** Fluorescence emission spectrum of DHC (2 μmol/L) in the presence of increasing
677 HSA concentrations (0-15 μmol/L) in PBS. **b** Fluorescence emission intensities of HSA
678 without DHC (I_{HSA}), DHC with HSA ($I_{DHC+HSA}$), and the difference of DHC+HSA and HSA
679 ($I_{DHC+HSA} - I_{HSA}$) (b; λ_{ex} = 325 nm, λ_{em} = 405 nm) (representative spectra and data)

680

681 **Fig. 3 a** Fluorescence emission spectrum of HSA (2 μmol/L) in the presence of increasing
682 DHC concentrations (0-4 μmol/L) in PBS (pH 7.4; λ_{ex} = 295 nm; representative spectra). **b**
683 Stern-Volmer plots of DHC-albumin (2 μmol/L albumin and 0-4 μmol/L DHC) complexes in
684 PBS (pH 7.4; λ_{ex} = 295 nm, λ_{em} = 340 nm; data were corrected based on Eq. 1) (representative
685 spectra and data)

686

687 **Fig. 4** Average CD spectra of native HSA (0.48 μmol/L) and (+)-DHC-HSA complex (each
688 0.48 μmol/L) after 5-h incubation in 30 mmol/L phosphate buffer (pH 7.4; representative
689 spectra)

690

691 **Fig. 5 a** The first four docked DHC conformations (Ranks 1-4) on HSA. **b** Detailed
692 presentation of Rank 4 DHC conformation surrounded by interacting amino acids of HSA

693

694 **Fig. 6 a** Fluorescence intensity of DHC and HSA (2 and 4 μmol/L, respectively) in the
695 presence of increasing concentrations of site marker (0-6 μmol/L) in PBS (pH 7.4; λ_{ex} = 325
696 nm, λ_{em} = 405 nm). **b** Fluorescence anisotropy values of ochratoxin A (1 μmol/L) in the

presence of HSA (1.5 μmol/L) and increasing concentrations of dihydrocitrinone (DHC), citrinin (CIT), and warfarin (WAR) (0-30 μmol/L each) in PBS (pH 7.4; λ_{ex} = 393 nm, λ_{em} = 446 nm). Data represent mean ± SEM (n = 3; * $p < 0.05$, ** $p < 0.01$)

Fig. 7 Effects of DHC (**a**) and CIT (**b**) on the ATP levels of MDCK cells after 24-hr incubation, in the absence and presence of FBS (10%) or HSA (40 g/L) (compared to the control: ** $p < 0.01$; compared to the effect without albumin: $^{\#}$ $p < 0.05$, $^{\#\#}$ $p < 0.01$). Data represent mean ± SEM (n = 3)

Tables

Table 1 Decimal logarithmic values of Stern-Volmer quenching constants (K_{SV}; unit: L/mol) and binding constants (K; unit: L/mol) of DHC-albumin complexes (see details in the "*Spectroscopic measurements*" section) Data represent mean ± SEM (n = 3)

Complex	logK_{SV} (± SEM) (Eq. 2, λ_{ex} = 295 nm)	log$K$ (±SEM) (Eqs. 3-7, λ_{ex} = 295 nm)	log$K$ (±SEM) (Eqs. 3-7, λ_{ex} = 325 nm)
DHC-HSA	4.68 ± 0.07	4.89 ± 0.03	5.51 ± 0.05
DHC-BSA	4.62 ± 0.07	4.75 ± 0.03	5.35 ± 0.02
DHC-PSA	4.45 ± 0.03	4.65 ± 0.01	4.93 ± 0.04
DHC-RSA	5.06 ± 0.00	5.30 ± 0.02	5.65 ± 0.02

DHC dihydrocitrinone, *HSA* human serum albumin, *BSA* bovine serum albumin, *PSA* porcine serum albumin, *RSA* rat serum albumin

Table 2 α-helix contents of HSA (0.48 μmol/L) and HSA after its incubation with (+)-DHC (both 0.48 μmol/L) in 30 mmol/L PBS (pH 7.4). α-helix percentage calculated with Eq. 10* and with the K2D3 software** (Louis-Jeune et al., 2012). Data represent mean ± SEM (n = 2)

HSA + (+)-DHC (ratio)	α-helix* (%)	α-helix ** (%)	relative difference
HSA	73.3 ± 0.3	67.4 ± 0.2	3-9%
HSA + (+)-DHC (1:1)	66.7 ± 0.5	65.7 ± 0.3	

DHC dihydrocitrinone, *CIT* citrinin, *HSA* human serum albumin

Figures:

Fig. 1

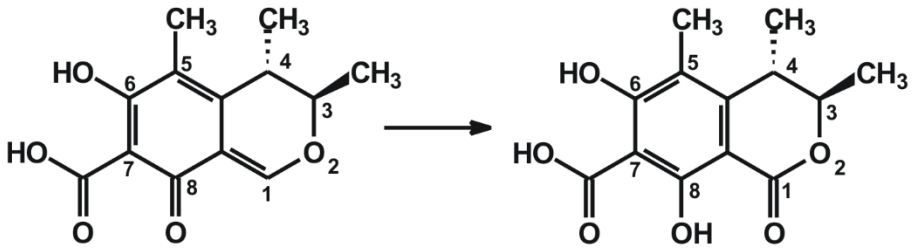

Fig. 2

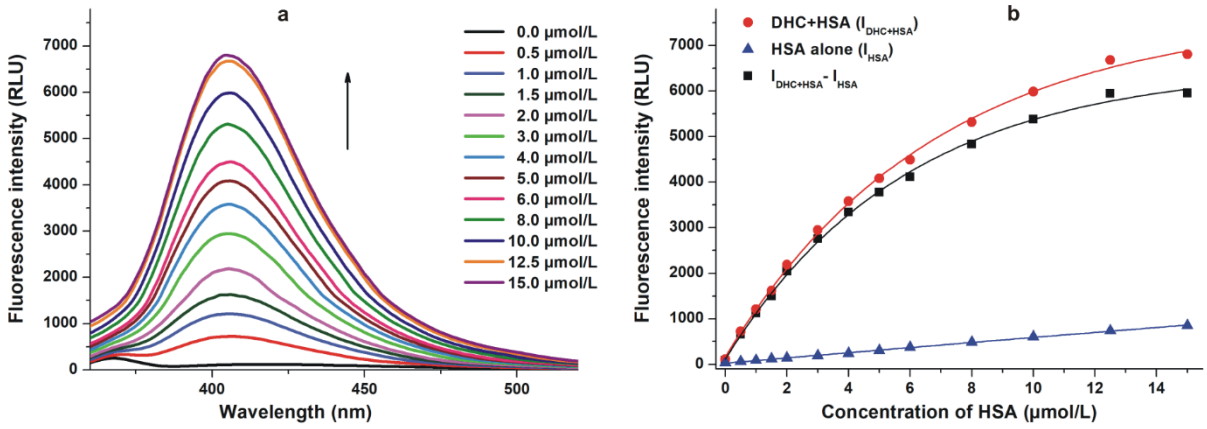

Fig. 3

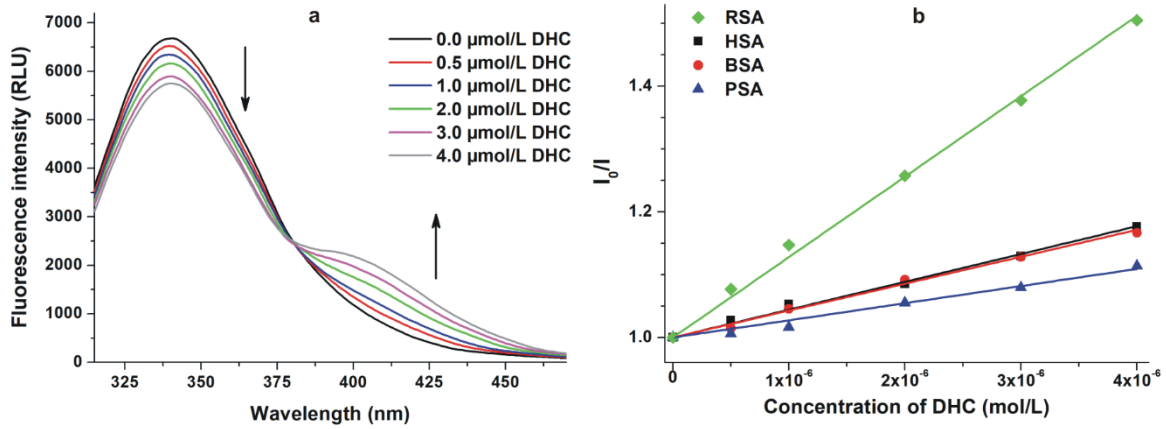

Fig. 4

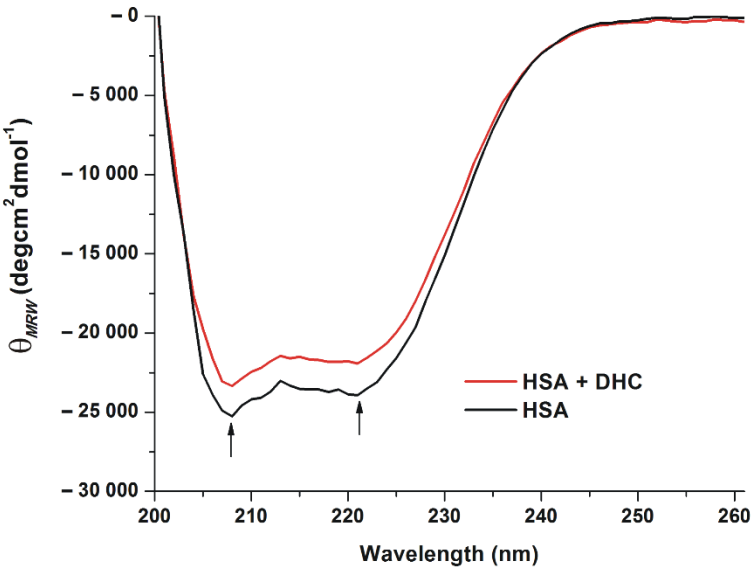
0
– 5 000
– 10 000
– 15 000
– 20 000
– 25 000
– 30 000
200
210
220
230
240
250
260
Wavelength (nm)
θMRW (degcm2dmol-1)
HSA + DHC
HSA

Fig. 5

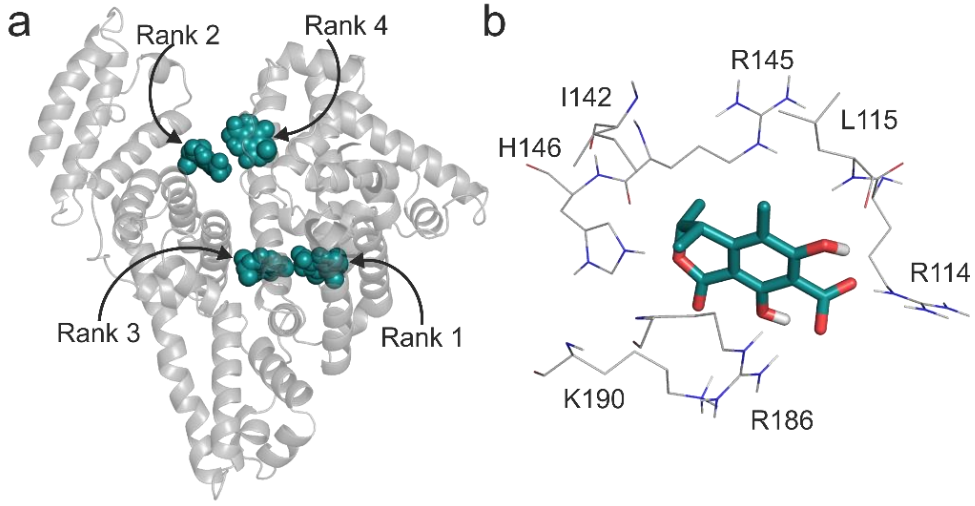
a
Rank 2
Rank 4
Rank 3
Rank 1
b
R145
I142
L115
H146
R114
K190
R186

744 ***Fig. 6***

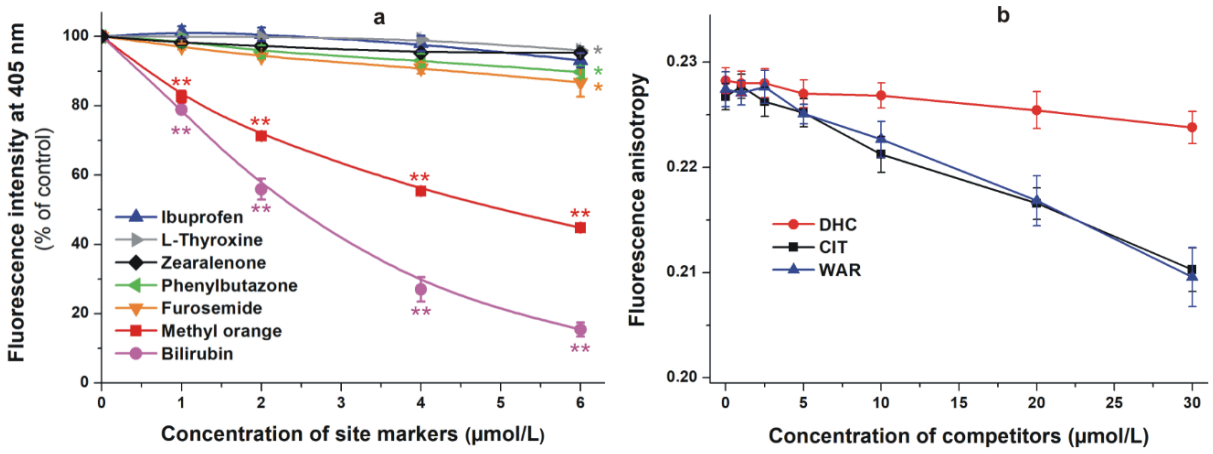

745

746

747

748 ***Fig. 7***

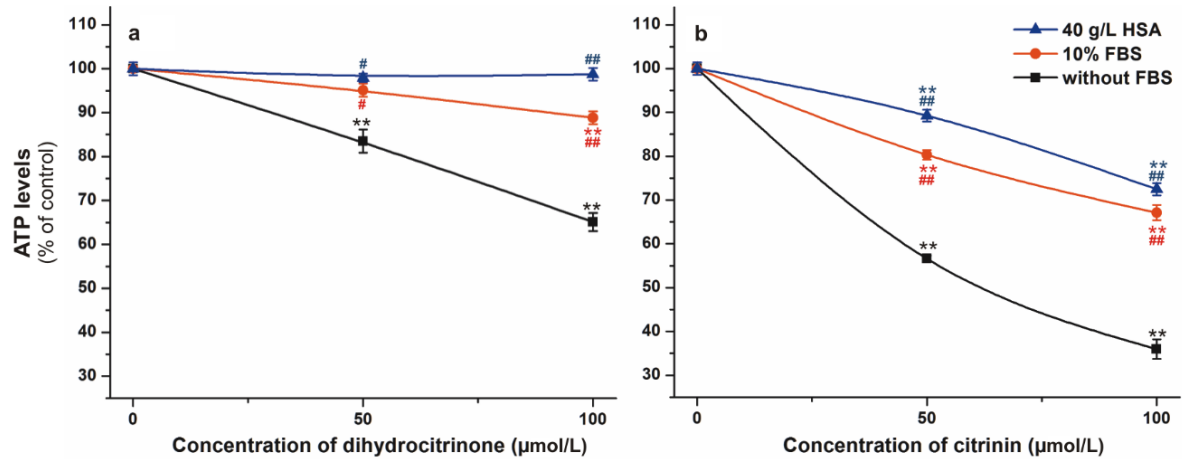

749